Jurnal Polimesin
Department of Mechanical Engineering
State Polytechnic of Lhokseumawe
http://e-jurnal.pnl.ac.id/polimesin

e-ISSN : 2549-1199 No. : 5 Month : October
p-ISSN : 1693-5462 Volume : 24 Year : 2026

Processing dates: received on 2026-8-04, reviewed on 2026-09-26, accepted on 2026-09-26 and online availability on 2026-10-31

Performance comparison of a modified lathe for rotary friction welding of steel and aluminum

Hudiyo Firmanto*, Thomas Widyatmoko, Prihartono, Misdi
Surabaya University, Gayungan, Surabaya, Jawa Timur 60231, Indonesia
*Corresponding author: hudiyo@staff.ubaya.ac.id

Abstract

Rotary friction welding (RFW) is a solid-state welding method that is very effective for joining dissimilar materials, but its application in research and educational laboratories is often limited by the high cost and complexity of dedicated RFW machines. To address this problem, this study aims to develop a practical and cost-effective electro-hydraulic actuation system that can be integrated with a conventional lathe to provide controlled axial loading for the RFW process, while allowing adjustment and control of the main process parameters. Three main components were designed and developed: a dedicated fixture to hold the joined specimen, a hydraulic power pack system to supply axial loads, and an electronic control unit for regulating axial force and dwell time. The system incorporates a double-acting hydraulic actuator with a 50 mm bore, a 150 mm stroke, and an operating pressure range of 3–200 bar. Welding trials were conducted using SS 304 stainless steel, AISI 1045 carbon steel, and Al 6061 aluminum alloy. The calculated welding efficiencies were 109.8%, 110.5%, and 69.7%, respectively. The efficiencies above 100% for SS 304 and AISI 1045 indicate that the welded specimens achieved higher tensile strengths than the corresponding base metals, whereas the lower efficiency for Al 6061 indicates reduced joint strength.

Keywords:
Rotary friction welding, electro-hydraulic actuation, conventional lathe, machine retrofit, solid-state welding

1 Introduction

Rotary Friction Welding (RFW) is a solid-state joining process primarily used to weld cylindrical components through rotational motion and axial pressure. Unlike conventional fusion welding, RFW joins materials without melting the interface, thereby offering the potential for reliable joints with reduced thermal effects and relatively short processing times. These characteristics make RFW particularly attractive for joining materials that are difficult to weld using conventional fusion processes, including dissimilar materials. Consequently, RFW has gained wide industrial and research applications due to its reliability and efficiency, being employed across sectors such as automotive, aerospace, machine tools, electronics, and heat exchangers [1-4]. The increasing interest in RFW also highlights the need for accessible and practical welding systems that can support both experimental research and educational activities, particularly in laboratories where the cost and complexity of dedicated RFW machines may limit their availability.

RFW relies on interfacial friction and axial compression to generate heat and form a metallurgical bond between the workpieces. The heat generated during friction, in combination with the material properties, strongly influences the joint quality. The bonding mechanism is primarily governed by interdiffusion and dynamic recrystallization occurring at the joint interface. The key process parameters in RFW include rotational speed, friction time, friction pressure, forging pressure, and forging time. Numerous studies have investigated the influence of these parameters on weld quality [5-10]. Therefore, the capability of an RFW machine to precisely control and vary these parameters is essential for conducting comprehensive experimental investigations.

Dedicated RFW machines are commercially available, as the process is widely used in industrial applications. However, such machines are typically very expensive. As an alternative, the RFW process has been successfully adapted for use with conventional machine tools—such as lathes and drill presses-through the addition of customized fixtures and pressing mechanisms. Several researchers have attempted to retrofit conventional lathes for RFW by integrating hydraulic or mechanical pressing systems [2], [11-18]. Nevertheless, achieving precise and repeatable control of axial pressure and timing remains a significant challenge. To address this limitation, the present study introduces an electro-hydraulic system equipped with electronic control for retrofitting a conventional lathe.

Recent retrofitting efforts implementing electro-hydraulic actuation have explored various approaches to enable RFW on conventional lathes: Candar *et al*. [14] implemented a PLC-based automation system with a direct-drive motor and hydraulic cylinder for compression, while Ta Van Ranh *et al.* [22] developed a lathe-based RFW machine equipped with a hydraulic cylinder for axial pressing, a kinetic braking mechanism, and laptop-based process control. Sunardi *et al.* [13] similarly employed a hydraulic system with a pressure gauge alongside a dedicated braking mechanism. Nevertheless, achieving precise and repeatable control of axial pressure and timing remains a significant challenge in these existing systems, as the control of hydraulic pressure and welding phase timing is either manually adjusted or managed through separate control modules, limiting the precision and repeatability of the transition between friction and forging stages. To address this limitation, the present study introduces a fully integrated electro-hydraulic actuation system with a unified electronic control circuit that governs both axial force and phase timing. This integrated approach ensures synchronized pressure delivery and timing accuracy throughout the entire welding cycle, offering a distinct improvement over previously reported retrofitted systems.

Therefore, the novelty of the proposed system lies in the integration of electronically controlled timing and electro-hydraulic actuation, enabling the axial pressure and welding sequence to be adjusted and reproduced more consistently than in conventional manually or mechanically controlled retrofit systems. This integrated control approach provides a practical means of improving parameter repeatability while retaining the low-cost and flexible nature of a conventional lathe-based RFW system. The developed setup enables repeatable and tuneable control of RFW parameters, providing a cost-effective and flexible platform for solid-state welding research and prototyping. This development bridges the gap between laboratory research and industrial practice by enabling precise control of RFW parameters using an accessible, retrofitted lathe-based system.

2 Research methodology

The RFW process is illustrated in Fig. 1. In this process, a non-rotating cylindrical specimen is pressed against a rotating one to generate interfacial pressure. This pressure is continuously applied to produce frictional heat at the contact interface between the specimens. Once sufficient heat is generated, rotation is stopped, and a forging pressure is applied to consolidate the joint. As shown in Fig. 1, the key RFW process parameters include rotational speed (N), friction pressure (P_f), friction time (T_f), forging pressure (P_u), and forging time (T_u).

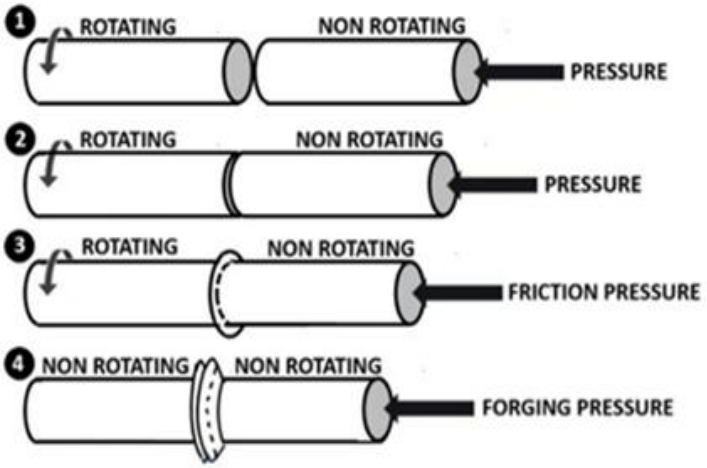


Fig. 1. RFW process

Based on the RFW process mechanism, this work retrofits a conventional lathe into an RFW system. A lathe inherently provides specimen holding and rotational motion; with the integration of auxiliary components-such as a fixture for the stationary specimen and a hydraulic system to supply axial force-the machine can be adapted to perform the friction and forging stages required in RFW. An electronic control circuit for the hydraulic system was developed to enable RFW operation under variable parameter settings.

The retrofitted system consists of four subsystems: (1) the stationary chuck and fixture, (2) hydraulic actuator, (3) hydraulic power unit, and (4) electronic control module. Each subsystem was designed to ensure coaxial alignment, controllable pressure, and repeatable motion. The design and configuration of the system are shown in Fig. 2.

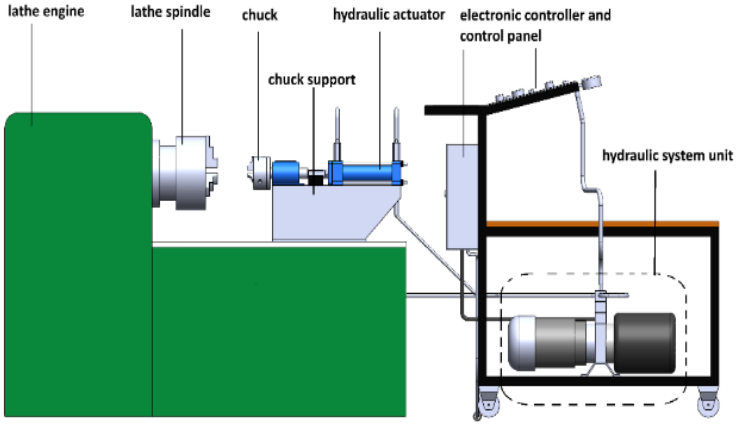


Fig. 2. Design and configuration of the ancillary hydraulic press system for the lathe machine

The design and development stages of the system are presented in Fig. 3. The design stage comprises three main development components: a fixture to hold the specimen, a hydraulic system, and an electronic control unit.

The fixture or stationary chuck was designed to hold a welding specimen of maximum 25 mm diameter. This was to be mounted on the lathe bed. The chuck support was required for positioning the hydraulic actuator that supplied axial pressure on the specimen to facilitate interfacial friction. This assembly could be dismantled at any time when the RFW system was not needed or when the machine was to be used for turning or machining work. Hydraulic pressure for the actuator was supplied by a hydraulic pump unit, which was installed separately from the machine. Subsequently, an electronic control system was developed to adjust and control the pressure and its application time.

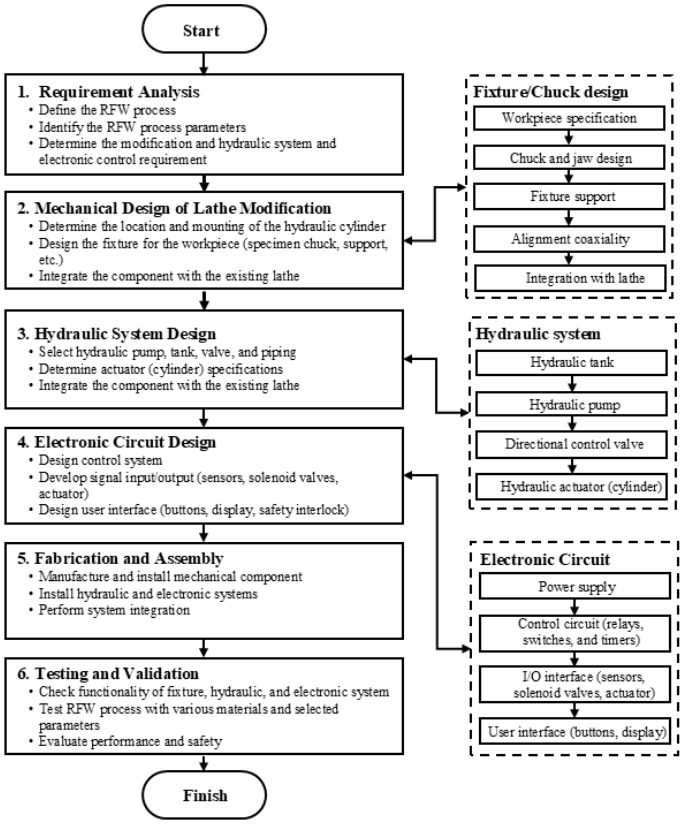


Fig. 3. Flowchart of the conventional lathe modification, hydraulic system, and electronic control integration for RFW.

3 Result and discussion

3.1 Chuck design

A stationary chuck (Fig. 4) was mounted on the lathe bed to hold the non-rotating specimen. It was designed to securely grip the specimen and prevent it from rotating due to friction with the rotating counterpart. The fixture must also be capable of withstanding axial pressure to maintain sufficient interfacial force between the two specimens. The chuck and spindle were aligned coaxially to ensure proper contact and load transfer. A bushing was incorporated to allow limited axial movement while maintaining angular rigidity. The design accommodates specimens with diameters ranging from 5 to 25 mm.

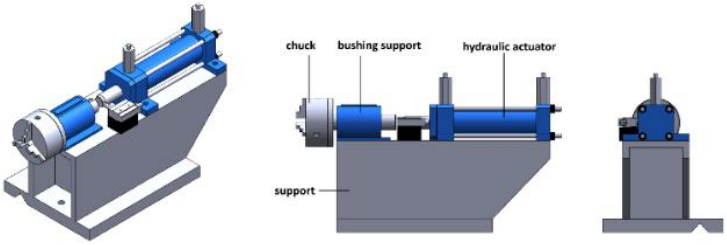


Fig. 4. Chuck assembly

3.2 Hydraulic actuation and control

A double-acting hydraulic actuator (50 mm bore, 150 mm stroke) applies the necessary axial load. The hydraulic system consists of a pump, reservoir, and control valves. The electric control unit manages solenoid valves and timers to regulate friction and forging phases.

Fig. 5 illustrates the schematic of the hydraulic circuit powering the axial actuator. The electric motor drives a hydraulic pump that supplies pressurized fluid to the system. Flow and direction are controlled by four-way directional valves, enabling the extension and retraction of the cylinder. Two parallel pressure relief valves with vent ports provide overpressure protection, while a filter ensures

fluid cleanliness. The circuit delivers stable hydraulic power, precise actuator control, and safe operation during the RFW process.

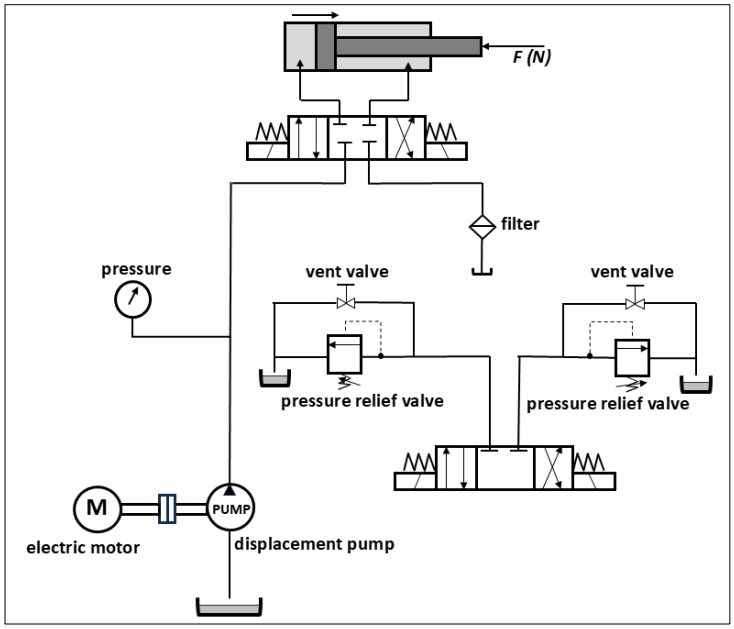


Fig. 5. Circuit diagram of the hydraulic system unit

An electric control circuit was designed to operate and regulate the hydraulic press, as shown in Fig. 6. The system comprises two main sections: the power circuit supplying energy to the hydraulic pump motor, and the control circuit managing operational sequences via relays, switches, and timers. The three-phase power system energizes the pump through the main contactor (*K-1*), while indicator lamps (*SLN* High, *SLN* Low, *SLN FWD*, *SLN BWD*) display pressure status and cylinder motion.

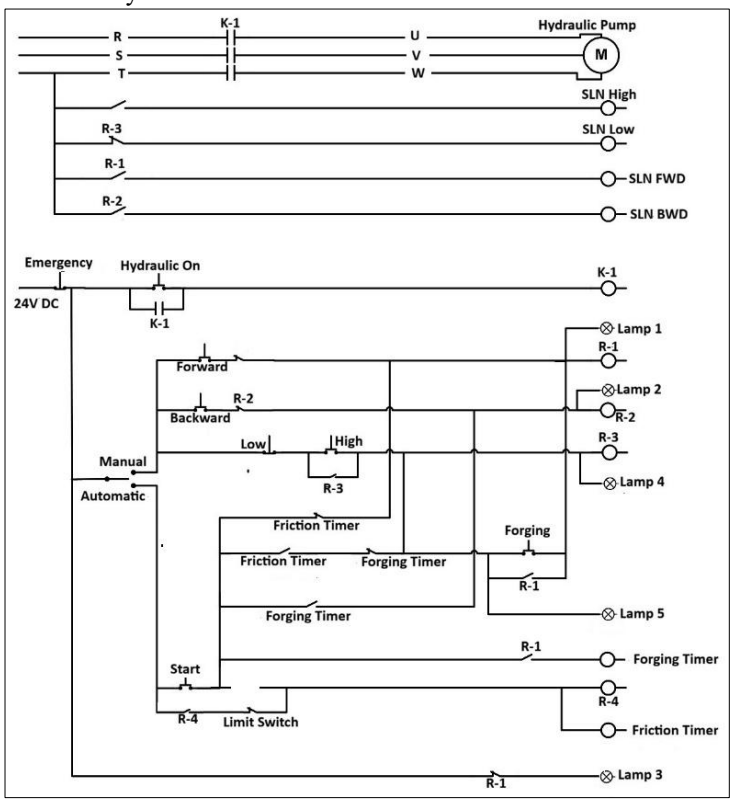


Fig. 6. Electronic control circuit of the pressure and time controller

The control section operates on a 24 VDC supply and incorporates an emergency-stop and hydraulic-on switch for safety. Relays *R-1* and *R-2* govern actuator movement with interlocking protection, and *R-3* selects between low- and high-pressure modes. Indicator lamps (*Lamp1–Lamp4*) provide visual feedback on relay status.

Pressure duration, a key parameter in the RFW process, is regulated by separate timers for the friction and forging phases, ensuring sequential operation. The forging timer activates relay *R-1*, energizing the solenoid to apply the required axial force, while relay *R-4* monitors stroke limits. Lamps (*Lamp5* and *Lamp3*) indicate the progression of each phase.

This integrated control design provides reliable, repeatable, and safe operation of the RFW process, enabling precise control over the friction and forging stages.

3.3 Analytical estimation of axial force and hydraulic pressure

Process parameters suggested from several RFW studies are summarized in Table 1 [19-24]. Those data were used as a basis to estimate the requirement of axial force and verify the suitability of the hydraulic actuator selection.

Table 1. Range of process parameters for RFW in various studies [19-24]

Parameter	Symbol	Typical Range	Unit
Rotational speed	N	800-2000	RPM
Friction pressure	P_f	60-120	Bar
Friction time	T_f	2-10	second
Forging pressure	P_u	100-200	Bar

The relation between welding pressure (friction or forging pressure), specimen diameter, axial force, and hydraulic pressure was calculated based on a simple equation, namely: $F = P.A$, where F = axial force, P = welding pressure (friction pressure/P_f or forging pressure/P_u), and A = cross-sectional area. In this calculation, the friction or forging pressures are assumed to act fully on the specimen cross-sectional area which is assumed to be in the form of a circle. It was also assumed that friction in the seal, pressure drop, as well as losses due to mechanical-system inefficiency are neglected in the stage of design estimation.

Axial force required for each specimen diameter is calculated using the aforementioned equation: $F_{axial} = P \times A_{specimen}$, with P being the applied welding pressure used in the calculation, and $A = \pi.(D^2/4)$ being the specimen cross-sectional area. The maximum welding pressure of 200 bar is employed based on the upper limit of the process parameters from previous studies, as given in Table 1. With this approach, the specimen diameter directly affects the axial force requirement. For the same welding pressure, an increase in specimen diameter causes the axial force to increase quadratically with the diameter.

The required hydraulic pressure is subsequently calculated based on: $P_{hydraulic}=F_{axial}/A_{actuator}$, where $A_{actuator}=\pi.(D^2_{actuator}/4)$, with $D_{actuator}= D_{bore}$ = 50 mm (bore diameter of the employed actuator). As an example, for the specimen diameter of 10 mm with the welding pressure of 200 bar, the estimated axial force is F_{axial} = 20 MPa X π ($10^2/4$) mm^2 =1.57 kN. With an actuator bore diameter of 50 mm, the hydraulic pressure is equal to $P_{hydraulic}$ =1.57 kN/ ($\pi.50^2/4$) mm^2 = 0.8 N/mm^2 = 0.8 MPa = 8 bar. Using a similar approach, the estimated axial force and hydraulic pressure for various diameters are shown in Table 2, while the relationship between the specimen diameter and both the axial force and hydraulic pressure is presented in Fig. 7.

Table 2. Axial force and actuator pressure required for RFW at various specimen diameters

Specimen Diameter (mm)	Axial Force (kN)	Hydraulic Pressure (bar)	Remarks
6	0.57	2.88	Suitable for aluminum and small steel bars
8	1.01	5.12	Standard range for RFW trials
10	1.57	8.00	Typical test specimen size
12	2.26	11.52	Medium force requirement
20	6.28	32.00	Much lower than the upper design limit of the selected actuator

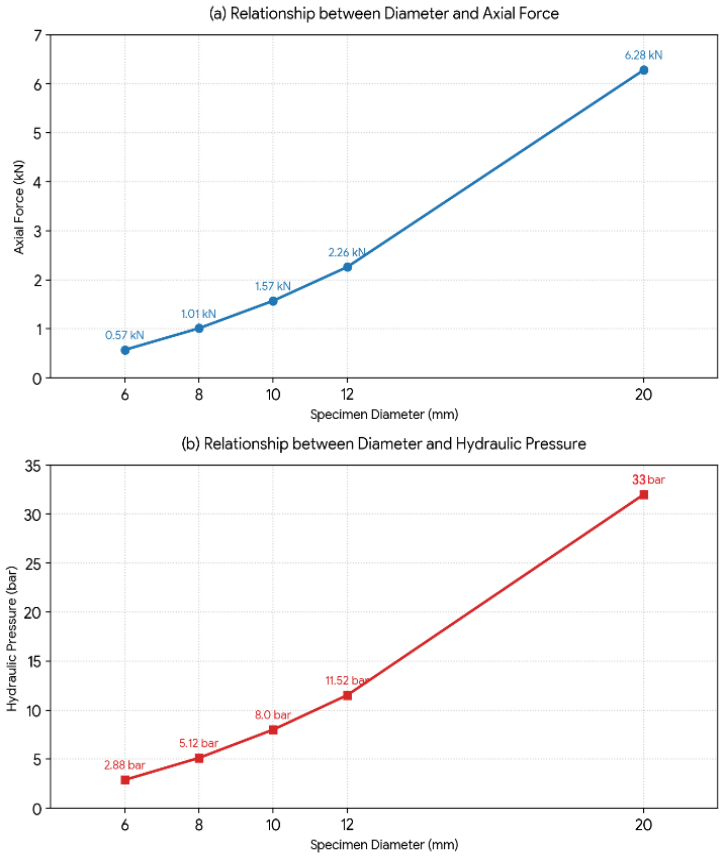


Fig. 7. Combinations of the axial force and actuator pressure required for welding specimens with various diameters

Fig. 7 (a) shows that the axial force grows as the specimen diameter increases. At the same welding pressure, a larger diameter leads to a larger cross-sectional area, so the required axial force also grows. For specimen diameters ranging from 6 to 20 mm, the required axial force rises from 0.57 to 6.28 kN. Fig. 7 (b) illustrates the relationship between the specimen diameter and the hydraulic pressure required by the actuator. The hydraulic pressure rises from 2.88 bar for a specimen diameter of 6 mm to approximately 33 bar for a diameter of 20 mm (the largest specimen diameter under consideration). This value is still far below the maximum working pressure of the actuator, which is 200 bar. This reveals that the selected actuator, with a working pressure range of 3–200 bar, is suitable for RFW under general operating conditions.

The developed RFW system is shown in Fig. 8. Fig. 8 (a) shows the chuck assembly and hydraulic actuation installed on the lathe bed, while the hydraulic pump and electronic control system are given in Fig. 8 (b).

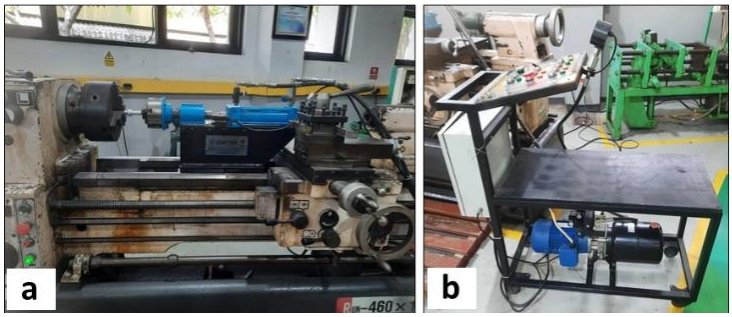


Fig. 8. Developed RFW system: (a) chuck assembly installed on the conventional lathe; (b) electro-hydraulic control unit.

A comparison of the developed system with previous works was carried out, and this is summarized in Table 3. As given in Table 3, previous research has employed various approaches to modify conventional machine tools into RFW machines. However, many of them developed only partial functionality, such as the use of hydraulic or pneumatic actuation, limited pressure adjustment and time control, and the absence of integrated electronic control. The present work develops a system which integrates adjustable hydraulic pressure and an electronic control system for forging and friction time. Validation of the welding results was also carried out. These efforts have addressed several limitations found in the previous work. Nevertheless, this system still has several limitations due to the absence of a load cell to measure the actual force at the interfacial contact of specimens, as well as a temperature monitoring system, which is frequently needed for RFW research. These features are important for advanced studies on process monitoring and parameter optimization and will be considered in future developments.

Table 3. Comparison of rotary friction welding machine development reported in previous studies and the present study

Study	Machine Base	Actuation System	Process Control	Pressure Adjustment	Time Control
Takhare *et al.* [11]	Conventional lathe	Hydraulic cylinder	No	Yes	Limited
Arun *et al.* [12]	Conventional lathe	Hydraulic hand pump	Manual	Yes	Limited
Sunardi *et al.* [13]	Conventional lathe	Hydraulic cylinder	No	Yes	Manual
Tran *et al.* [15]	Self-designed machine	Hydraulic cylinder	Solenoid	Yes	Yes
Çandar *et al.* [14]	Idle lathe	Hydraulic cylinder	Automation	Yes	Yes
Dellepiane *et al.* [36]	Drill press	Calibrated loading system	Electronic monitoring	Yes	Yes
This study	Modified Conventional lathe	Electro-hydraulic actuator	Electronic controller	Yes	Yes

3.4 Welding trials

The machine was tested to join ferrous and non-ferrous alloys, *i.e.*, carbon steel (AISI 1045), stainless steel (SS 304), and aluminum (Al 6061). The metals were in the form of 16 mm diameter rods. Welding samples were prepared from the rods with a length of 120 mm. The RFW process was conducted using the parameters shown in Table 4. Subsequently, tensile testing and inspection of the joint macrostructure were carried out to evaluate the welding results.

Table 4. Experimental parameters used in machine trials

Metals	Rotation speed (RPM)	Friction pressure (bar)	Friction time (sec.)	Forging pressure (bar)	Forging time (sec.)
SS 304	1330	90	7	100	3
AISI 1045	1330	90	7	100	3
Al 6061	1330	20	7	60	3

The results of the machine trials on the materials are shown in Fig. 9. Each joining was repeated twice to assess the consistency of the machine. Two repetitions of the welding trials were applied, considering the typical number of replications commonly used in welding experiments. For efficiency, this number of repetitions was considered sufficient. The form of the flash at the joint and the burn length are indications of the joining consistency. Visually, the welds for all materials showed good results. A uniform flash at the joint indicated a sound joint. The joints of ferrous alloys (*i.e.*, SS 304 and AISI 1045) as well as Al 6061 exhibited good quality, and the samples of the materials showed good concentricity of the welded parts.



Fig. 9. RFW joint sample of SS 304, AISI 1045, and Al 6061

Fig. 9 demonstrates that, visually, sound joints were formed across all three materials. Flash formed at the joint interface is regular and significant in size, indicating effective deformation and joining processes. These results also show that, at the selected parameter settings, the friction generated sufficient heat to soften the material, enabling deformation and joining to occur. Visual inspection also reveals good concentricity across the three joints. The symmetrical shape of the flash indicates that the samples underwent uniform compression; in other words, the sample holders—both the lathe spindle chuck and the actuator unit chuck—gripped the samples securely without slippage during the joining process.

To further examine the physical quality of the joints, an observation of the joint cross section was carried out. The macrostructure of the RFW joints of SS 304, AISI 1045, and Al 6061 is presented in Fig. 10 – 12. Macroscopically, all joints indicate a continuous joint formation with a clear and regular flash around the interface zone. In SS 304 and AISI 1045, the area around the interface demonstrates a relatively finer morphological change from the base metal towards the interface. This can generally be related to the thermo-mechanically affected zone (TMAZ/TMZ) and the heat affected zone (HAZ). However, further study on this reaction zone is not performed since this is beyond the scope of this work. In Al 6061, the changes in material shape and flash appear more prominent, which implies a larger plastic flow during the RFW process. Overall, the existence of the deformation zone and the flash, which are formed continuously adjacent to the interface, is an indication that contact, friction, heating, and plastic deformation during the RFW process have taken place effectively and subsequently produce a well-formed joint. The cross-sectional images of the joints across all three materials also demonstrate good specimen concentricity, confirming that the specimen positioned in the custom-built chuck was aligned coaxially with the material mounted on the spindle.

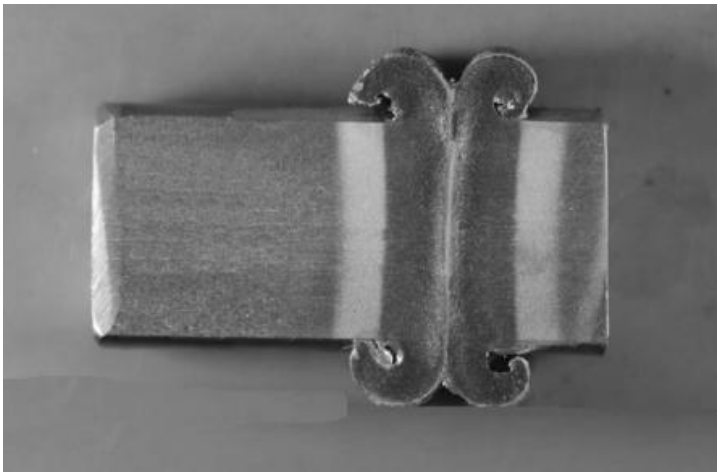


Fig. 10. Macrostructure of cross section of the SS 304 RFW joint

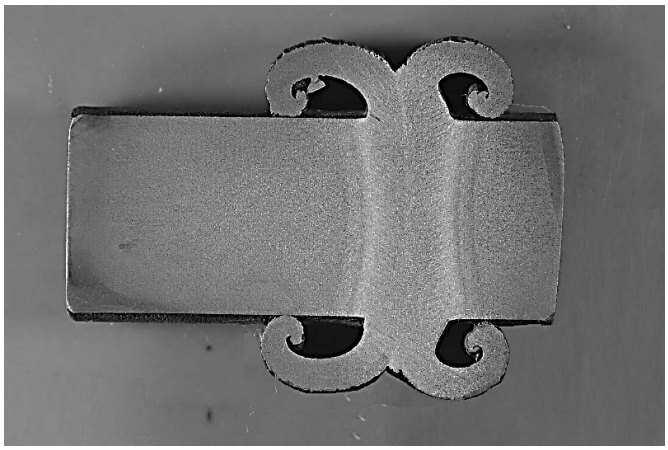


Fig. 11. Macrostructure of cross section of the AISI 1045 RFW joint

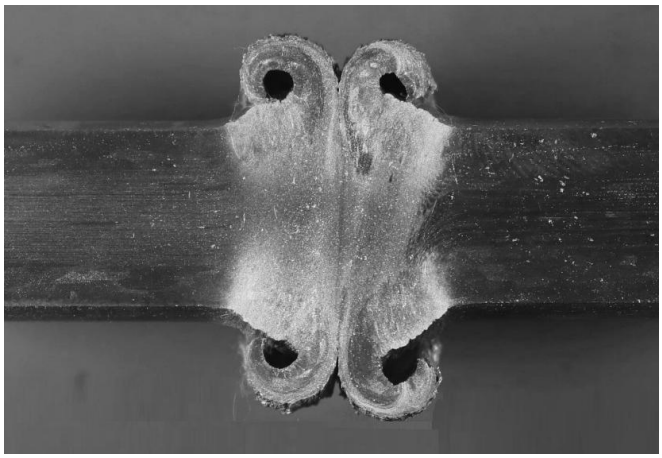


Fig. 12. Macrostructure of cross section of the Al 6061 RFW joint

To evaluate the joint strength, tensile tests were performed on all the joints. Prior to the tensile test, the joined metals were machined into tensile test specimens according to ASTM E8. The test results are given in Table 5. To assess the quality of joint strength quantitatively, the welding efficiency of the joint is calculated. Prior to joining, each base metal underwent tensile testing. The resulting tensile strength served as a benchmark for the welded joint strength and was used to calculate the welding efficiency. Welding efficiency, or tensile strength efficiency, is the ratio of the joint strength to the tensile strength of the base metal prior to joining [17, 24–29]. This terminology is a common metric for evaluating welding quality in the field of welding. Besides tensile strength and welding efficiency, the burn-off length that occurs during welding is also measured. This is the shortening of the welded specimen due to the axial force and plastic deformation during the process, and can be an indicator of the amount of deformed material caused by heating and axial pressure. Tensile strength, welding efficiency, and the measured burn-off length are given in Table 5. Subsequently, for better comparison, the data in Table 5 are presented in the chart shown in Fig. 13.

The tensile test results show that for the ferrous alloys (*i.e.*, SS 304 and AISI 1045), the tensile strength of the joint samples is higher than that of the base metal. The tensile strength data given in Table 5 gives the welding efficiency of 109.8%, 110.5%, and 69.7% for SS 304, AISI 1045, and Al 6061, respectively. Thus, the welding efficiency for the steels exceeds 100%, while for the aluminum, the welding efficiency is below 100%.

Table 5. Tensile strength, welding efficiency and burn-off length

	UTS (MPa)		Welding Efficiency (%)	Burn of Length (mm)
	Base Metal	RFW Joint		
SS 304	699.51	768.51	109.8	8.5
AISI 1045	706.54	780.95	110.5	32.7
Al 6061	369.24	257.47	69.7	22.9

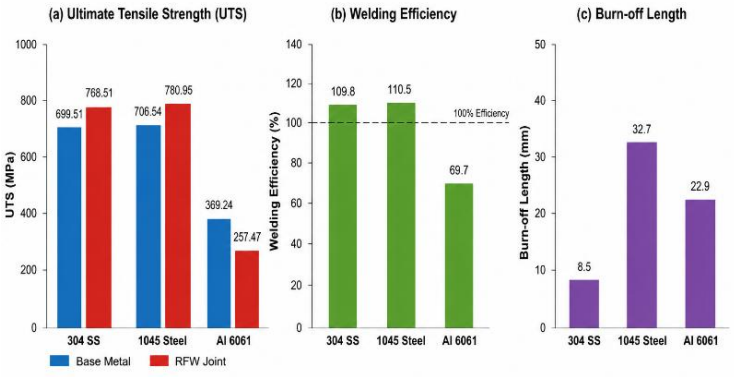


Fig. 13. Mechanical and process characteristics of RFW joints: (a) ultimate tensile strength (UTS) of base metal and RFW joints; (b) welding efficiency; (c) burn-off length

Generally, the joint region is often the weakest region of a welded component due to the thermal effects associated with the welding process. A welding efficiency exceeding 100%, as observed in the experimental results, indicates that the tensile strength of the welded specimen is higher than that of the corresponding base metal. This is further supported by the fracture occurring outside the joint region, indicating that the joint region was not the weakest part of the tested specimens. In RFW, this improvement in joint strength may be associated with strain hardening induced by the severe plastic deformation during welding. In addition, grain refinement associated with dynamic recrystallization at the joint interface may contribute to the improvement in hardness and strength. These mechanisms have been reported in previous studies on the RFW of steel [17, 24, 27]. The welding efficiencies of 109.8% and 110.5% obtained using the developed equipment are within, or even higher than, the range reported in previous studies on the rotary friction welding of ferrous alloys [17, 24-29]. Thus, the developed system is capable of performing experiments for research purposes in the field of RFW.

Different results were obtained for the Al 6061 joint. The tensile strength of the joint was 257.47 MPa, which was lower than that of the base metal (369.24 MPa), resulting in a welding efficiency of 69.7%. This result aligns with previous studies [30–35]. Compared to the steels, the welding efficiency of aluminum was lower, which can be attributed to several factors, primarily oxide formation and the thermal softening effect. Previous studies have reported that the formation of aluminum oxide (Al_2O_3) could contribute to the low strength of the joint compared to its base metal [19]. The oxide, which is easily formed during aluminum welding, can weaken the joint interface layer. Additionally, the lower melting temperature of aluminum can cause significant thermal softening at the interface during the friction process [37, 38]. Thus, although the interface successfully bonds, the region around the joint becomes weaker than the base metal.

The tensile test results revealed that the retrofitted lathe machine can produce welded joints with mechanical performance comparable to those produced by conventional RFW machines.



Fig. 14. Fractured tensile-test specimen of the SS 304, AISI 1045, and AL 6061 RFW joint

The tensile strength results obtained from the tests are consistent with the fracture locations of the tensile specimens. As shown in Fig. 14 (fractured tensile–test specimens), fracture during the tensile test occurred in the base metal, which indicates that the joints are of good quality.

The burn-off length during welding varies significantly among the materials. AISI 1045 steel produces the highest burn-off length, followed by Al 6061 and SS 304 (see Fig. 13). This difference may reflect each material's thermophysical characteristics: localized heat in AISI 1045 stimulates massive plastic deformation, whereas Al 6061 is restrained by high heat dissipation and self-lubrication. Conversely, the minimum burn-off length of SS 304 implies good mechanical resistance and microstructural stability at high temperature.

The overall trial results revealed that the developed system can produce a high-quality RFW joint of SS 304, AISI 1045, and aluminum (Al 6061). Observations of the welded joints, macrostructure of the joint, the tensile test results, and the welding efficiency demonstrated the effectiveness of the retrofitted lathe machine for the rotary friction welding process. The machine successfully joined both ferrous and non-ferrous alloys. Further evidence of the quality of the welded joints could be obtained through microstructural and hardness examination of the weld interface. However, such metallographic analyses are beyond the scope of the present study and will be considered for future work.

4 Conclusion

This study developed and evaluated an RFW system integrated with a conventional lathe. The lathe spindle provides specimen rotation, while the hydraulic system supplies axial loading with dedicated fixture for specimens up to 25 mm in diameter. For a 20 mm diameter specimen, the required hydraulic pressure was approximately 33 bar, still within the actuator operating range. Welding trials on 16 mm diameter SS 304, AISI 1045, and Al 6061 specimens were conducted at 1330 rpm using material-specific friction and forging pressures. The measured joint tensile strengths were 780.95 MPa, 768.51 MPa, and 257.47 MPa, respectively, compared with 706.54 MPa, 699.51 MPa, and 369.24 MPa for the corresponding base metals. The calculated welding efficiencies were 109.8% for SS 304, 110.5% for AISI 1045, and approximately 69.7% for Al 6061. These results indicate that the welded steel specimens exceeded the tensile strength of their base metals, whereas the aluminum joints exhibited lower tensile strength. The results demonstrate the potential of the modified lathe for RFW of small-diameter metallic rods. Future improvements should include a load cell for real-time axial force measurement and a temperature sensor to monitor the thermal cycle, enabling better process control and further optimization of welding parameters.

Acknowledgement

The authors would like to express their sincere gratitude to the Directorate of Resources, Ministry of Higher Education, Science, and Technology, Republic of Indonesia, which funded this work through the 2024 Laboratory Staff Innovation Grant Program No. 087/KILab/E4/DT.04.03/2024.

References

[1] T. D. Kannan, P. Sivaraj, V. Balasubramanian, S. Malarvizhi, T. Sonar, M. Ivanov, and S. Sathiya, "Joining Different Grades of Low Carbon Steel to Develop Unsymmetrical Rod to Plate Joints Using Rotary Friction Welding for Automotive Applications," Forces in Mechanics, vol. 10, article no. 100153, 2023, https://doi.org/10.1016/j.finmec.2022.100153

[2] V. Ajay, N. K. Babu, M. Ashfaq, T. M. Kumar, and K. V. Krishna, "A Review on Rotary and Linear Friction Welding of Inconel Alloys," Trans Indian Inst Met., vol. 74, no. 11, pp. 2583–2598, 2021, doi: 10.1007/s12666-021-02345-z.

[3] R. Pardeshi, P. Patil, S. Surashe, P. Shinde, and P. V. V. Kulkarni, “Recent Industrial Scenario of Rotary Friction Welding Technology and Its Applications- A Review,” The International Journal for Research in Engineering Application & Management, vol. 5, pp. 196–199, 2019.
[4] D. G. Hattingh, M. N. James, F. K. Schwim, R. Opperman, D. Bernard, and I. Wedderburn, “Innovative Rotary Friction Welding of Heat Exchanger Tube Nozzles on High Pressure Headers,” International Journal of Pressure Vessels and Piping, vol. 210, article no. 105263, 2024, doi: 10.1016/j.ijpvp.2024.105263.
[5] M. Maalekian, “Friction Welding - Critical Assessment of Literature,” Science and Technology of Welding and Joining, vol. 12, no. 8, pp. 738–759, 2007, doi: 10.1179/174329307X249333.
[6] P. Gaikwad, S. Naik, N. Dhutre, S. Maniyar, and V. Kulkarni, “Parametric Analysis of Rotary Friction Welding Process Based on Comparative Study between Mild Steel and Stainless Steel 304,” International Journal for Research in Engineering Application & Management (IJREAM), vol. 5, no. special issue, pp. 224–228, 2019.
[7] D. K. Thirumalaikkannan, S. Paramasivam, S. Murugesan, and B. Visvalingam, “Effect of Rotational Speed on The Microstructure and Mechanical Properties of Rotary Friction Welded AISI 1018/AISI 1020 Asymmetrical Joints,” Material Testing, vol. 64, no. 11, pp. 1561–1571, 2022, doi: 10.1515/mt-2022-0188.
[8] H. E. Lakache, R. Badji, and A. May, “Parametric Investigation of Similar TiAl6V4 and AA2024 Rotary Friction Weld Joints Using Taguchi-L9 Array Method,” Iranian Journal of Materials Science and Engineering, vol. 20, no. 3, 2023, doi: 10.22068/ijmse.3121.
[9] H. Firmanto, S. Candra, and M. A. Hadiyat, “Rotary Friction Welding of 304 Stainless Steel: Parametric Study, Mechanical Properties, and Microstructure of The Joint,” J. Polimesin, vol. 22, no. 2, p. 191, 2024, doi: 10.30811/jpl. v22i2.4978.
[10] M. D. Kumar and P. Savitharoja, “Parametric Effects on Mechanical and Metallurgical Properties of Rotary Friction Welded UNS S30400 & UNS S31803 Tubes,” International Journal of Innovative Research in Technology, vol. 10, no. 5, pp. 328–331, 2023.
[11] P. A. Thakare and L. R. Singh, “Design and Development of Micro Friction Welding Machine and Investigation of Welding Parameters for Similar Materials,” International Journal of Scientific & Engineering Research, vol. 5, no. 6, pp. 1379–1384, 2014, [Online]. Available: http://www.ijser.org
[12] P. B. Arun, N. K. Raj, V. Yadhu, and C. S. Sanalkumar, “To Design and Construct a Friction Welding Attachment on Lathe, Conduct Experiment and to Study about Mechanical Behavior of Friction Welded Joints of Aluminum Rods,” International Journal of Engineering Research & Technology (IJERT), vol. 6, no. 7, pp. 150–158, 2017, doi: 10.17577/ijertv6is070113.
[13] A. Sunardi, M. Mariyana, A. Gamayel, M. N. Mohammed, and M. Zaenudin, “Design & Development of Friction Welding Machine Based on Lathe Machine,” AIP Conference Proceedings 2578, 070002, 2022.
[14] H. Çandar, S. Olguner, A. Abra, and Y. E. Çimen, “Conversion and Automation of An Idle Lathe into A Rotary Friction Welding Experimental System,” Turkish Journal of Electromechanics and Energy, vol. 48, no. 2, pp. 43–48, 2024.
[15] T. V. Hung, T. V. Ranh, T. T. V. Nga, and L. H. Ky, “Research and Test of the Self-Designed and Manufactured Rotary Friction Welding Machine with CT3 Steel Samples,” Engineering Innovations, vol. 3, pp. 23–34, 2022, doi: 10.4028/p-rod566.
[16] S. Suhadi, and R. Tuhumena, “Friction Welding Machine Design,” Proceeding of International Joint Conference on UNESA, PIJCU, vol. 2, no. 2, pp. 1–8, 2025, [Online]. Available: https://proceeding.unesa.ac.id/index.php/pijcu
[17] M. A. Marir, E. L. Sheng, I. O. Bachi, and M. R. Isa, “Tensile Efficiency and Fatigue Life of Similar and Dissimilar Carbon Steel Joints Subjected to Rotary Friction Welding,” Journal of Advanced Joining Processes, vol. 8, 2023, doi: 10.1016/j.jajp.2023.100168.
[18] A. A. Mattie, S. Y. Ezdeen, and G. I. Khidhir, “Optimization of Parameters in Rotary Friction Welding Process of Dissimilar Austenitic and Ferritic Stainless Steel Using Finite Element Analysis,” Advances in Mechanical Engineering, vol. 15, no. 7, pp. 1–16, 2023, doi: 10.1177/16878132231186015.
[19] H. Ghari, A. Taherizadeh, B. Sadeghian, B. Sadeghi, and P. Cavaliere, “Metallurgical Characteristics of Aluminum-Steel Joints Manufactured by Rotary Friction Welding: A Review and Statistical Analysis,” Journal of Materials Research and Technology, vol. 30, pp. 2520–2550, 2024, https://doi.org/10.1016/j.jmrt.2024.03.089
[20] M. S. Owis, S. Z. El-Abden, A. A. Abd-Eltwab, and K. M. A. A. Elkader, “Rotary Friction Welding of Aluminum Alloy Tube to Tube with Edge Using External Tool,” Journal of Engineering Sciences, vol. 52, no. 5, pp. 120–135, 2024, doi: 10.21608/jesaun.2024.258411.1298.
[21] R. Das, G. Sivaswamy, H. Lalvani, and A. P. Singh, “Fracture Toughness and Microstructural Analysis of Rotary Friction Welded S355J2 And SS316L Steels for Critical Applications,” Journal of Advanced Joining Processes, vol. 10, article no. 100244, 2024, doi: 10.1016/j.jajp.2024.100244.
[22] T. V. Ranh, L. H. Ky, V. Duong, and T. D. Thuan, “Evaluation of Technical Specifications of Rotary Friction Welding Machine Improved from Lathe,” Advances in Transdisciplinary Engineering, vol. 58, pp. 80–86, 2024, doi: 10.3233/ATDE240607.
[23] L. Huihong, C. Kailiang, W. Zexi, L. Yongbi, and Y. Morisada, “A Novel Multi-Stage Pressuring Strategy to Fabricate Sound High-Carbon Steel Joints in Rotary Friction Welding,” Journal of Manufacturing Processes, vol. 133, pp. 957–968, 2025, https://doi.org/10.1016/j.jmapro.2024.11.101
[24] M. Farbakhti, S. R. E. Hosseini, S. A. M. Mohammadi, S. Sadatabhari, Y. M. Huo, and R. Li, “Similar and Dissimilar Rotary Friction Welding of Steels: A Review of Microstructural Evolution and Mechanical Properties,” Journal of Materials Research and Technology, vol. 36, pp. 8777–8803, 2025, doi: 10.1016/j.jmrt.2025.05.079.
[25] V. A. Alza, “Mechanical Properties and Microstructure, in welded joints of Low and Medium Carbon Steels, Applying Rotary Friction,” International Journal of Recent Technology and Engineering (IJRTE), Volume-8, Issue-6, pp. 5176–5185, March 2020.
[26] M. Iswar and R. Nur, “Effect of Friction Welding Conditions on Tensile Strength and Hardness of AISI 310 Stainless Steel Joints,” MATEC Web of Conferences 204, 06004 (2018); https://doi.org/10.1051/matecconf/201820406004.
[27] Z. S. Tawfeeq and R. H. Gardi, “Mechanical Properties and Microstructure of Rotary Friction Welded Super Duplex Stainless Steel Pipe,” Zanin Journal of Science and Engineering, vol 1, no.3, pp. 111–121, 2025, https://doi.org/10.64362/zjse.942025.
[28] S. T. Selvamani, K. Palanikumar, K. Umanath, and D. Jayaperumal, “Analysis of Friction Welding Parameters on the Mechanical Metallurgical and Chemical Properties of AISI 1035 Steel Joints,” Materials and Design, vol. 65, pp. 652–661, 2015.
[29] A. Tokarev, A. Yakhin, and D. Karetnikov, “Evaluation of Efficiency of Rotary Friction Welding in Obtaining Joints from Corrosion and Heat-Resistant Steel,” E3S Web of Conferences 525, 03005, 2024.

[30] T. Teker, T. Soysal, and G. Akgün, “Efecto De La Soldadura Por Fricción Rotativa Sobre Las Propiedades Mecánicas De La Aleación Al 6060,” Revista de Metalurgia, vol. 57, no. 4, e206, 2021, doi: 10.3989/revmetalm.206.
[31] L. H. Eddine, M. Abdelghani, and B. Riad, “Rotary Friction Welding Parameters Effects upon Mechanical Properties and Microstructure of AA2024 Weld Joints,” Engineering Solid Mechanics, vol. 11, pp. 291-298, 2023, doi: 10.5267/j.esm.2023.2.003
[32] P. Hariprasath, P. Sivaraj, and V. Balasubramanian, “A Critical Assessment on Rotary Friction Welded High Strength Armor Grade Aluminum Alloy Joints,” Physics of Metals and Metallography, 2021, doi: 10.1134/S0031918X21130044.
[33] T. Jantarasricha, S. Kunhirunbawon, and M. Wimol, “Investigation of Optimum Parameters for Rotary Friction Welding of Aluminum Round Bars Using Three-Level Factorial Design Methodology,” Journal of Metals, Materials, and Minerals, vol. 31, no. 4, pp. 88–94, 2021, doi: 10.14456/jmmm.2021.62.
[34] H. Khalid, S. Arshad, A. Mumtaz, A. Farooq, and M. Ishfaq, “Experimental and Finite Element Analysis of Rotary Friction Welded Aluminum Rods,” International Conference on Advances in Civil and Environmental Engineering 2024. University of Engineering & Technology, Taxila Pakistan, pp. 238–247.
[35] M. A. Tashkandi, and M. I. Mohamed, “Effect of Friction Time on the Mechanical and Microstructural Properties of AA6061 Joints by Continuous Drive Friction Welding,” Engineering, Technology & Applied Science Research, vol. 10, no. 3, pp. 5596–5602, 2020.
[36] M. Dellepiane, L. Da Silva, and A. Toumpis, “Design and Development of a Bespoke Rotary Friction Welding Machine in Exploration of Joining Dissimilar Materials for Nuclear Applications,” Journal of Manufacturing and Materials Processing, vol. 9, no. 27, 2025, https://doi.org/10.3390/jmmp9010027
[37] A. Sasmito, M. N. Ilman, and P. T. Iswanto, “Effects of Rotational Speed on The Mechanical Properties and Performance of AA6061-T6 Aluminium Alloy in Similar Rotary Friction Welding,” Welding International, vol. 37, no. 9, pp. 519–530, 2023, https://doi.org/10.1080/09507116.2023.2265811
[38] A. Kalinenko, K. Kim, I. Vysotskiy, I. Zuiko, S. Malopheyev, S. Mironov, and R. Kaibyshev, “Microstructure-Strength Relationship in Friction-Stir Welded 6061-T6 Aluminum Alloy,” Materials Science and Engineering: A, vol. 793, 2020, https://doi.org/10.1016/j.msea.2020.139858